

## Direct Probe of Topological Invariants Using Bloch Oscillating Quantum Walks

V. V. Ramasesh,<sup>1</sup> E. Flurin,<sup>1</sup> M. Rudner,<sup>2</sup> I. Siddiqi,<sup>1</sup> and N. Y. Yao<sup>1</sup>

<sup>1</sup>Department of Physics, University of California, Berkeley California 94720, USA

<sup>2</sup>Niels Bohr International Academy and Center for Quantum Devices, University of Copenhagen, 2100 Copenhagen, Denmark

(Received 18 November 2016; published 27 March 2017)

The topology of a single-particle band structure plays a fundamental role in understanding a multitude of physical phenomena. Motivated by the connection between quantum walks and such topological band structures, we demonstrate that a simple time-dependent, Bloch-oscillating quantum walk enables the direct measurement of topological invariants. We consider two classes of one-dimensional quantum walks and connect the global phase imprinted on the walker with its refocusing behavior. By disentangling the dynamical and geometric contributions to this phase, we describe a general strategy to measure the topological invariant in these quantum walks. As an example, we propose an experimental protocol in a circuit QED architecture where a superconducting transmon qubit plays the role of the coin, while the quantum walk takes place in the phase space of a cavity.

DOI: 10.1103/PhysRevLett.118.130501

**Introduction.**—Much like their classical stochastic counterparts, discrete-time quantum walks [1] have stimulated activity across a broad range of disciplines. In the context of computation, they provide exponential speedup for certain oracular problems and represent a universal platform for quantum information processing [2–4]. Quantum walks also exhibit features characteristic of a diverse set of physical phenomena, ranging from localization to molecule formation [5,6]. At their core, discrete-time quantum walks (DTQW) are dynamical protocols associated with spinful particles on a lattice, where the internal spin state controls the direction of motion [5–19]. Motivated by this intrinsic spin-orbit coupling, a tremendous body of recent work has focused on exploring the topological features of DTQWs both theoretically and experimentally [5,11–15].

A connection between quantum walks and topology has been made by mapping the unitary evolution of the DTQW protocol to stroboscopic evolution under an effective Hamiltonian. In certain cases—distinguished by a combination of symmetry and dimensionality—the effective Hamiltonian’s band structure exhibits a quantized invariant, analogous to those found in topological insulators [5,11,12,14]. On one hand, these invariants have helped to enable a sharp classification of noninteracting topological phases, which, unlike conventional symmetry-breaking phases, do not exhibit any local order parameter [20,21]. On the other, they underlie a multitude of exotic physical phenomena ranging from protected edge modes and quantized conductance to fractional charges and magnetic monopoles [22,23]. Despite their importance and owing to their *nonlocality*, bulk topological invariants have been directly probed in only a handful of quantum optical systems [24–27] and a generic blueprint for their measurement remains an outstanding challenge.

In this Letter, we demonstrate that the simulation platform associated with discrete-time quantum walks is

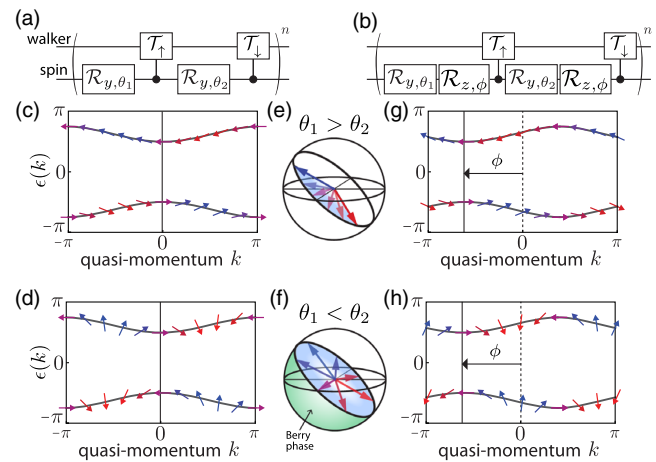


FIG. 1. The sequence of unitary operations associated with a single step of (a) the split-step quantum walk and (b) the Bloch-oscillating quantum walk. (c) The band structure and spin texture (arrows accompanying the band) for a trivial split-step quantum walk [ $U_{SS}(3\pi/4, \pi/4)$ ] with  $W = 0$  and (d) for a topological split-step quantum walk [ $U_{SS}(\pi/4, 3\pi/4)$ ] with  $W = 1$ . (e), (f) Schematic evolution of the spin eigenvectors in (c),(d) as one traverses the Brillouin zone. In the topological phase, the spin texture fully winds around the origin as  $k$  varies from  $[-\pi, \pi]$ . (g), (h) Analogous band structures for the trivial and topological Bloch-oscillating quantum walk. The shift in the effective momentum induced by the  $z$  rotations (by  $\phi$ ) are shown explicitly.

naturally suited for the direct extraction of topological invariants. We analyze a time-dependent, “Bloch-oscillating” generalization of two classes (split-step and single-step) of one-dimensional DTQWs. In these protocols, a geometric signature of the topological invariant is imprinted as a Berry phase on the quantum state of the particle. We demonstrate that this phase can be extracted and disentangled from other contributions via a simple

interferometric protocol [28,29]. Our results directly connect to previous seminal observations of the refocusing behavior of time-dependent quantum walks [30–32] and provide a physical explanation for such behavior in terms of dynamical and geometric phases. While our approach is general, we propose an experimental realization in a circuit quantum electrodynamics architecture, leveraging the use of cavity Schrödinger cat states to directly measure the topological invariant via Wigner tomography.

*General approach.*—Let us begin by considering the family of protocols, dubbed split-step quantum walks, which act on a single spin-1/2 particle ( $\{|\downarrow\rangle, |\uparrow\rangle\}$ ) in a one-dimensional lattice  $\{|x\rangle, x \in \mathbb{Z}\}$  [5]. Parametrized by angles  $\theta_1$  and  $\theta_2$ , these protocols consist of a sequence of unitary operations [Fig. 1(a)]: (i) a spin rotation  $R_y(\theta_1) = e^{-i\theta_1\sigma_y/2}$ , (ii) a spin-dependent translation  $T_\uparrow = \sum_x [|x+1\rangle\langle x| \otimes |\uparrow\rangle\langle\uparrow| + |x\rangle\langle x| \otimes |\downarrow\rangle\langle\downarrow|]$ , (iii) a second spin rotation  $R_y(\theta_2)$ , and (iv) a second spin-dependent translation  $T_\downarrow = \sum_x [|x\rangle\langle x| \otimes |\uparrow\rangle\langle\uparrow| + |x-1\rangle\langle x-1| \otimes |\downarrow\rangle\langle\downarrow|]$  [5,12,33]. Denoted  $U_{SS}(\theta_1, \theta_2)$ , this sequence comprises a single step of the quantum walk.

Although the protocol is defined in discrete unitary steps, the subsequent evolution can be related to that produced by an effective Hamiltonian,  $H_{\text{eff}}$  (at stroboscopic times), where  $e^{-iH_{\text{eff}}} = U_{SS}(\theta_1, \theta_2)$ . In the quasimomentum basis  $|k\rangle = (1/\sqrt{2\pi})\sum_x e^{-ikx}|x\rangle$ , the spin-dependent translation operators are diagonal ( $T_\uparrow = e^{ik(\sigma_z-1)/2}$  and  $T_\downarrow = e^{ik(\sigma_z+1)/2}$ ), and thus,

$$H_{\text{eff}} = \epsilon_{\theta_1, \theta_2}(\hat{k}) \mathbf{n}_{\theta_1, \theta_2}(\hat{k}) \cdot \boldsymbol{\sigma}, \quad (1)$$

where  $\hat{k} = \int dk |k\rangle\langle k|$ ;  $\epsilon_{\theta_1, \theta_2}(k)$  characterizes the band structure; and  $\mathbf{n}_{\theta_1, \theta_2}(k)$  specifies the corresponding spinor eigenstate [Figs. 1(c),(d)]. An underlying chiral symmetry of  $U_{SS}$  constrains  $\mathbf{n}(\hat{k})$  to lie on a great circle of the Bloch sphere [34]. The number of times,  $W$ , which  $\mathbf{n}(\hat{k})$  winds around the origin as  $k$  varies from  $[-\pi, \pi]$  defines the topological invariant of the walk [5,10,13]. Depending on  $\{\theta_1, \theta_2\}$ , the split-step quantum walk mimics motion either in a trivial band with winding number zero or a topological band with winding number unity [Figs. 1(e),(f)] [35]. A key signature of this topological invariant is the geometric Berry phase,  $\phi_{\text{geo}} = \pi W$ , acquired by the particle's wave function upon an adiabatic traversal through the Brillouin zone.

In order to imprint this Berry phase on the wave function of the quantum walker, we consider a time-dependent modification to  $U_{SS}$ , aimed at generating dynamics analogous to solid-state Bloch oscillations [30,31]; the modified  $m^{\text{th}}$  step unitary [Fig. 1(b)] is

$$U_{SS}^{(m)}(\theta_1, \theta_2) = T_\downarrow R_z(-m\phi) R_y(\theta_2) T_\uparrow R_z(-m\phi) R_y(\theta_1), \quad (2)$$

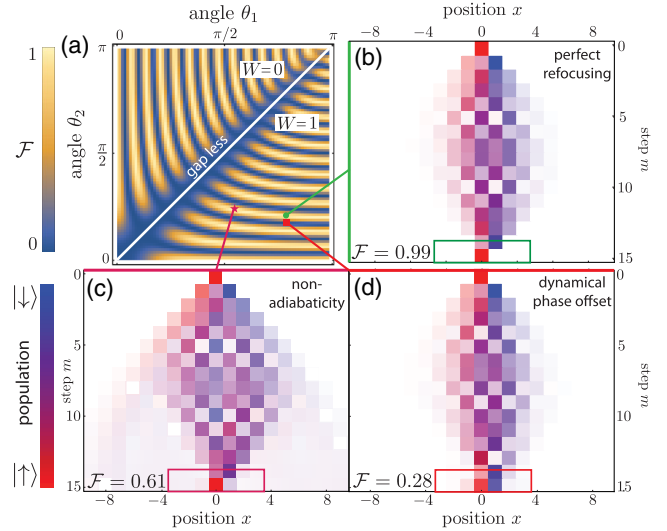


FIG. 2. (a) Refocusing fidelity  $\mathcal{F} = |\langle \psi_0 | \psi_f \rangle|^2$  computed from numerical simulations of an  $N = 30$  step Bloch-oscillating quantum walk as a function of  $\{\theta_1, \theta_2\}$ , where  $\phi = 2\pi/N$ . Two topologically distinct regions  $W = 0$  ( $\theta_1 > \theta_2$ ) and  $W = 1$  ( $\theta_1 < \theta_2$ ) are separated by a gapless line. In the vicinity of this gap closure, the refocusing fidelity drops dramatically owing to nonadiabatic transitions. The observed stripe pattern in the refocusing fidelity follows the contour lines for which the accumulated dynamical phase is a multiple of  $\pi$ . (b)–(d) Three specific time evolutions associated with various  $\{\theta_1, \theta_2\}$ : (b) a perfectly refocusing walk, (c) a nonrefocusing walk due to nonadiabatic transitions, and (d) a nonrefocusing walk due to an accumulated dynamical phase of  $\pi/2$ .

where  $R_z(-m\phi) = e^{i\sigma_z m\phi/2}$  and  $\phi = 2\pi/N$  for  $N \in \mathbb{Z}$ . Since  $T_\uparrow R_z(-m\phi) = e^{im\phi/2} e^{i(\hat{k}+m\phi)(\sigma_z-1)/2}$  and  $T_\downarrow R_z(-m\phi) = e^{-im\phi/2} e^{i(\hat{k}+m\phi)(\sigma_z+1)/2}$ , the additional  $z$  rotations simply shift the original quasimomentum by a step-dependent amount and result in a modified effective Hamiltonian,

$$\hat{H}_{\text{eff}}^{(m)} = \epsilon_{\theta_1, \theta_2}(\hat{k} + m\phi) \mathbf{n}_{\theta_1, \theta_2}(\hat{k} + m\phi) \cdot \boldsymbol{\sigma}. \quad (3)$$

In the limit  $\phi \ll 1$ , this shift defines an adiabatic translation of momentum space, where the quantum walker traverses the full Brillouin zone in precisely  $N$  steps.

To understand the dynamics of the “Bloch-oscillating” quantum walk, we map the discrete evolution associated with the series of step-dependent unitaries,  $U_{SS}^{(m)}$ , to continuous evolution under a time-dependent Schrödinger equation:  $i\partial_t |\psi\rangle = H_{\text{eff}}(\hat{k} + \Delta k(t)) |\psi\rangle$ , where  $H_{\text{eff}}(\hat{k} + \Delta k(t))$  captures the step-dependent effective Hamiltonian in Eq. (3) via  $\Delta k(t) = \phi \sum_m \Theta(t - m)$ , where  $\Theta$  is the Heaviside step function.

The analogy to Bloch oscillations is best captured by moving into a nonuniformly accelerating frame via the

transformation,  $U_{\Delta k(t)} = e^{i\hat{x}\Delta k(t)}$ , wherein the state,  $|\tilde{\psi}\rangle = U_{\Delta k(t)}^\dagger |\psi\rangle$  satisfies

$$i\partial_t |\tilde{\psi}\rangle = \left( H_{\text{eff}}(\hat{k}) + \hat{x}\phi \sum_m \delta(t-m) \right) |\tilde{\psi}\rangle. \quad (4)$$

The above time evolution mirrors that of a particle on a stationary lattice receiving periodic kicks of magnitude  $\phi$  and the resulting dynamics resemble Bloch oscillations.

To see this, let us consider an initial state  $|\tilde{\psi}(0)\rangle = |k\rangle \otimes |\mathbf{n}_k^\pm\rangle$ , where  $|\mathbf{n}_k^+\rangle$  and  $|\mathbf{n}_k^-\rangle$  are the spinor eigenstates (at momentum  $k$ ) of the upper and lower bands (Fig. 1), respectively. For  $\phi \ll 1$ , the adiabatic theorem allows one to explicitly solve Eq. (4) [33],

$$|\tilde{\psi}(t)\rangle = e^{i\phi_{\text{dyn},\pm}} e^{i\phi_{\text{geo},\pm}} |k+m\phi\rangle |\mathbf{n}_{k+m\phi}^\pm\rangle. \quad (5)$$

The momentum and spinor eigenstates simply follow their adiabats while the overall wave function acquires both a dynamical and geometric phase,

$$\begin{aligned} \phi_{\text{dyn},\pm} &= \pm \sum_{m \geq 0} \epsilon(k+m\phi), \\ \phi_{\text{geo},\pm} &= i\phi \sum_{m \geq 0} \langle \mathbf{n}_{k+m\phi}^\pm | \partial_k \mathbf{n}_{k+m\phi}^\pm \rangle. \end{aligned} \quad (6)$$

Since  $|k+2\pi\rangle |\mathbf{n}_{k+2\pi}^\pm\rangle = |k\rangle |\mathbf{n}_k^\pm\rangle$ ,  $|\tilde{\psi}(m)\rangle$  exhibits a recurrence to its initial state—up to a global phase—whenever  $m/N$  is an integer [30,31]; this is precisely analogous to Bloch oscillations, in which Bloch waves recover their initial momentum upon any full traversal of the Brillouin zone.

This recurrence forms the basis of our protocol to measure topological invariants in quantum walks. By performing an interference measurement (e.g., Ramsey spectroscopy) between the refocused wave function,  $|\tilde{\psi}(m)\rangle$ , and a reference state, one can directly extract the overall global phase  $\phi_T = \phi_{\text{dyn}} + \phi_{\text{geo}}$ . As will be shown below, it is possible to disentangle the dynamical and geometric contributions to  $\phi_T$  by simply varying the overall step number. In this way, one can extract  $\phi_{\text{geo}}$ , thereby directly measuring the topological winding number.

Although recurrence always occurs for initial momentum or spinor eigenstates (e.g.,  $|\tilde{\psi}(0)\rangle = |k\rangle \otimes |\mathbf{n}_k^\pm\rangle$ ), quantum walks are typically initialized with the particle localized at a single initial site. As such states consist of superpositions of eigenstates in both the upper and lower energy bands,

$$|\tilde{\psi}(0)\rangle = \sum_k c_k |k\rangle |\mathbf{n}_k^+\rangle + d_k |k\rangle |\mathbf{n}_k^-\rangle, \quad (7)$$

their refocusing behavior is significantly more subtle, requiring not only that each constituent eigenstate return to itself, but also that the total accrued phase is identical for all components. While the geometric phase acquired after  $N$  steps is  $\pi W$  for all eigenstates, the dynamical phase acquired

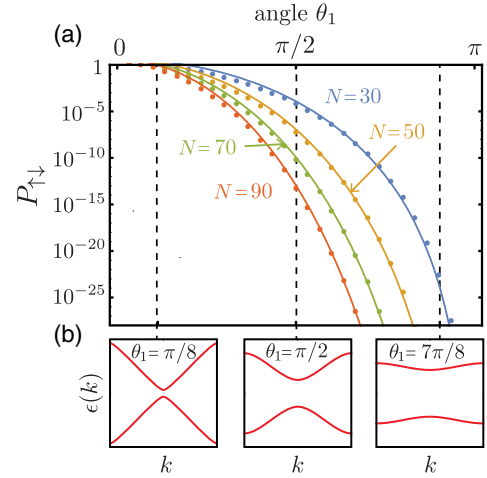


FIG. 3. (a) Nonadiabatic transition probability as a function of  $\theta_1$  for the single-step quantum walk ( $\theta_2 = 0$ ). Solid lines correspond to analytic formulas derived in Ref. [31], which capture the deviations from ideal refocusing behavior. Points correspond to  $P_{\uparrow\downarrow}$  as computed from Eq. (9), demonstrating that the physical origin of such deviations is nonadiabatic Landau-Zener transitions. (b) Schematic band structures for various  $\theta_1$ . The band gap increases as  $\theta_1$  varies from 0 to  $\pi$  leading to a smaller nonadiabatic transition probability.

by states in the upper and lower bands are opposite [Eq. (6)]. Thus, the final state will generally *not* refocus to the initial state [Fig. 2(a)] and the wave function will remain spread over a number of sites [Fig. 2(d)].

Fortunately, one can always ensure near-perfect refocusing (i.e., enforcing a dynamical phase which is arbitrarily close to a multiple of  $2\pi$  [36]) by first characterizing the fidelity as a function of total step number. In particular, in the limit of large step number, the dynamical phase becomes proportional to  $N$ :  $\phi_{\text{dyn}} \approx N \times \bar{\epsilon}$ , where  $\bar{\epsilon} = \int dk \epsilon(k)/2\pi$  [37]. The refocusing fidelity,  $\mathcal{F} = |\langle \psi_0 | \psi_f \rangle|^2$ , is then given by [33]

$$\mathcal{F} = \cos^2(N\bar{\epsilon}), \quad (8)$$

enabling one to control the refocusing via a choice of  $N$ ; this is illustrated by the perfectly refocused state in Fig. 2(b), where the global phase contains only the geometric component.

In addition to dynamical phase accumulation, nonadiabatic transitions can also lead to a lack of refocusing. This is particularly evident near regions where the gap closes as one transitions from a topological to trivial band structure. In such cases, even when  $\phi_{\text{dyn}} \propto 2\pi$  [38], the refocusing fidelity can be imperfect owing to interband Landau-Zener transitions [Fig. 2(c)].

To quantify this effect, we consider single-step Bloch-oscillating quantum walks [ $\theta_2 = 0$  in Eq. (2)]. As shown in Fig. 3, the effective band structure of the quantum walk changes as one varies  $\theta_1$ , with the band gap increasing

continuously as  $\theta_1$  varies from 0 to  $\pi$ . An enhanced gap should decrease the nonadiabatic transition probability  $P_{\uparrow\downarrow}$ , which can be explicitly computed for  $\phi \ll 1$  as [33]

$$P_{\uparrow\downarrow} \approx \phi^2 \left| \sum_{m=1}^N \langle \mathbf{n}_{k+m\phi}^- | \partial_k \mathbf{n}_{k+m\phi}^+ \rangle e^{-2i \sum_{p=0}^m \epsilon(k+p\phi)} \right|^2. \quad (9)$$

One finds that  $P_{\uparrow\downarrow}$  is in quantitative agreement with analytics on single-step Bloch-oscillating quantum walks (Fig. 3) [30,31,33]. As in the case of dynamical phase accumulation, one can tune the number of steps  $N$  to minimize nonadiabatic refocusing errors below any desired threshold.

So far we have shown how to construct a Bloch-oscillating quantum walk from an arbitrary split- or single-step quantum walk. By choosing the number of steps  $N$  such that the state of the particle is refocused, one finds that the final wave function differs from the initial state by only an imprinted geometric phase, which encodes the topology of the quantum walk. While global phases are generally unmeasurable, below we show how this geometric phase can be extracted interferometrically in a system with an additional internal state.

*Experimental realization.*—We now propose an experimental blueprint for extracting topological invariants from Bloch-oscillating quantum walks in a circuit quantum electrodynamics (cQED) architecture [39]. We consider a superconducting transmon qubit [40] coupled to a high-quality-factor electromagnetic cavity [Fig. 4(a)] and envision the quantum walk to take place in the phase space of the cavity mode [41]. Each lattice site corresponds to a particular coherent state of the cavity and the two logical states of the transmon ( $|g\rangle$ ,  $|e\rangle$ ) form the internal spin of the walker [42].

Spin rotations  $R_y(\theta)$  and  $R_z(\phi)$  can be performed using coherent microwave driving, with state-of-the-art pulse shaping techniques enabling single-qubit  $X$  and  $Y$  Clifford gates with greater than 99.9% fidelity in as little as 20 ns [43]. Spin-dependent translations arise naturally from the dispersive coupling between the qubit and the cavity,  $H_{\text{int}} = \hbar(\chi/2)a^\dagger a \sigma_z$  [Fig. 4(b)] [44]. Here,  $\sigma_z$  is the Pauli  $z$  operator of the transmon qubit,  $a^\dagger$  ( $a$ ) the cavity raising (lowering) operator, and  $\chi$  the strength of the qubit-cavity dispersive coupling.

In combination, the above operations enable the realization of a quantum walk on a circular lattice in cavity phase space [Fig. 4(c)]. In particular, one initializes the cavity in a coherent state  $|\alpha\rangle$ , with the qubit in the ground state  $|g\rangle$ . After applying the desired unitary rotation to the qubit, a waiting period of time  $t$  allows the dispersive interaction to naturally implement the spin-dependent translation. Indeed, a coherent state  $|\alpha\rangle$  in the cavity frame precesses either clockwise ( $|\alpha\rangle|e\rangle \rightarrow |\alpha \exp(i\chi t/2)\rangle|e\rangle$ ) or counterclockwise ( $|\alpha\rangle|g\rangle \rightarrow |\alpha \exp(-i\chi t/2)\rangle|g\rangle$ ) depending on the qubit state [Figs. 4(b), (c)]. Choosing  $t$  such that  $\chi t = 2\pi/L$  defines the  $L$  coherent state “lattice sites”:  $\{|\alpha \exp(i2\pi\ell/L)\rangle, \ell \in [0, L-1]\}$ .

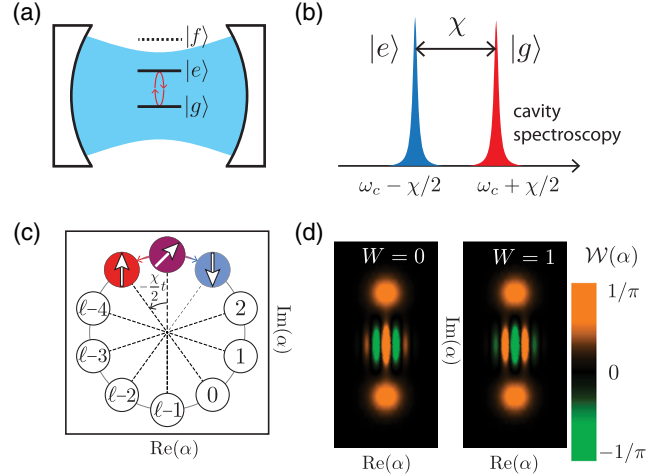


FIG. 4. (a) Schematic of the proposed cQED setup for realizing Bloch-oscillating quantum walks, utilizing a superconducting cavity mode coupled to a transmon qubit. The levels  $|g\rangle$ ,  $|e\rangle$  form the internal spin states of the walker, while  $|f\rangle$  is used as a shelving state. (b) The qubit and cavity couple dispersively, realizing a state-dependent shift of the bare cavity transition frequency  $\omega_c$  that naturally enables spin-dependent translations. (c) The quantum walk takes place on a circular lattice in the phase space of the cavity. Each coherent state depicted in the figure represents a particular lattice site of the walk. Spin-down (-up) corresponds to state  $|g\rangle$  ( $|e\rangle$ ). (d) Wigner tomography  $\mathcal{W}(\alpha)$  of the cavity following a refocused Bloch-oscillating quantum walk in the topological and trivial band structures reveals the underlying winding number in the phase of the interference fringes.

These two basic steps (unitary rotation and spin-dependent translation) can then be repeated to realize a Bloch-oscillating quantum walk. Measurement of the quantum walker’s spin and position after each step can be performed via full tomography of the cavity-qubit system [45].

To directly probe the topological invariant via the imprinted geometric phase, one must perform interferometry between the refocused wave function and a reference state. This is naturally enabled by the proposed cQED architecture, where one can initialize the system in a cavity Schrödinger cat state, corresponding to a coherent superposition,  $1/\sqrt{2}(|\alpha\rangle|g\rangle + |0\rangle|f\rangle)$ , where  $|0\rangle$  is the vacuum state of the cavity and  $|f\rangle$  is the second excited state of the qubit. Crucially, the  $|0\rangle|f\rangle$  state behaves as a phase reference since it is immune to both the unitary spin rotations and the dispersive coupling. The  $|f\rangle$  state in transmon qubits can exhibit coherence and decay times in excess of 20  $\mu\text{s}$  [46], while the aforementioned pulse-shaping techniques result in off-resonant leakage errors  $< 10^{-5}$ .

Upon refocusing of the  $|\alpha\rangle|g\rangle$  component, the final wave function takes the form  $1/\sqrt{2}(e^{i\pi W}|\alpha\rangle|g\rangle + |0\rangle|f\rangle)$  and the topological winding number manifests in the geometric relative phase between the two components. After disentangling the spin and cavity degrees of

freedom via number-selective qubit pulses (i.e.,  $|0\rangle|f\rangle \rightarrow |0\rangle|g\rangle$ ) [47], one can perform full Wigner tomography of the cavity state. As illustrated in Fig. 4(d), the resulting interference patterns display fringes whose phase corresponds to  $\pi W$  [45,48].

In summary, we have demonstrated that the simulation platform associated with quantum walks can enable the direct measurement of bulk topological invariants. In particular, by constructing Bloch-oscillating analogues of both split- and single-step quantum walks, we have introduced an interferometric protocol to directly measure the winding number associated with a quantum walk's effective band structure. A key feature of such Bloch-oscillating quantum walks is their natural refocusing behavior, whose microscopic origin arises from an interplay between dynamical and geometric phases as well as non-adiabatic transitions. Looking forward, our results can be directly extended to measurements of quantum walk topological invariants in higher dimensions, and provide a bridge toward probing many-body invariants associated with interacting quantum walks.

We gratefully acknowledge the insights of and discussions with E. Demler, L. Martin, S. Hacohe-Gourgy, and C. Navarrete-Benlloch. This research is supported in part by the Miller Institute for Basic Research in Science, the Laboratory Directed Research and Development Program of Lawrence Berkeley National Laboratory under U.S. Department of Energy Contract No. DE-AC02-05CH11231, the U.S. Army Research Office (ARO) under Grant No. W911NF-15-1-0496 and by the AFOS under Grant No. FA9550-12-1-0378. M.R. gratefully acknowledges the Villum Foundation and the People Programme (Marie Curie Actions) of the European Unions Seventh Framework Programme (FP7/2007-2013) under REA Grant Agreement No. PIFI-GA-2013-627838 for support. V.V.R. acknowledges funding from an NSF graduate research fellowship.

- 
- [1] S.E. Venegas-Andraca, *Quantum Inf. Process.* **11**, 1015 (2012).
- [2] E. Farhi and S. Gutmann, *Phys. Rev. A* **58**, 915 (1998).
- [3] A. Ambainis, *SIAM J. Computing* **37**, 210 (2007).
- [4] A.M. Childs, *Phys. Rev. Lett.* **102**, 180501 (2009).
- [5] T. Kitagawa, M. S. Rudner, E. Berg, and E. Demler, *Phys. Rev. A* **82**, 033429 (2010).
- [6] P.M. Preiss, R. Ma, M.E. Tai, A. Lukin, M. Rispoli, P. Zupancic, Y. Lahini, R. Islam, and M. Greiner, *Science* **347**, 1229 (2015).
- [7] A. Nayak and A. Vishwanath, [arXiv:quant-ph/0010117](https://arxiv.org/abs/quant-ph/0010117).
- [8] A.M. Childs and J. Goldstone, *Phys. Rev. A* **70**, 022314 (2004).
- [9] H. Obuse, J.K. Asbóth, Y. Nishimura, and N. Kawakami, *Phys. Rev. B* **92**, 045424 (2015).
- [10] C. Cedzich, F.A. Grünbaum, C. Stahl, L. Velzquez, A.H. Werner, and R.F. Werner, *J. Phys. A* **49**, 21LT01 (2016).
- [11] T. Kitagawa, M. A. Broome, A. Fedrizzi, M. S. Rudner, E. Berg, I. Kassal, A. Aspuru-Guzik, E. Demler, and A. G. White, *Nat. Commun.* **3**, 882 (2012).
- [12] T. Kitagawa, *Quantum Inf. Process.* **11**, 1107 (2012).
- [13] J. K. Asbóth and H. Obuse, *Phys. Rev. B* **88**, 121406 (2013).
- [14] J. K. Asbóth, *Phys. Rev. B* **86**, 195414 (2012).
- [15] B. Tarasinski, J. K. Asbóth, and J. P. Dahlhaus, *Phys. Rev. A* **89**, 042327 (2014).
- [16] M. Karski, L. Förster, J.-M. Choi, A. Steffen, W. Alt, D. Meschede, and A. Widera, *Science* **325**, 174 (2009).
- [17] F. Zähringer, G. Kirchmair, R. Gerritsma, E. Solano, R. Blatt, and C. F. Roos, *Phys. Rev. Lett.* **104**, 100503 (2010).
- [18] A. Schreiber, K. N. Cassemiro, V. Potoček, A. Gábris, P. J. Mosley, E. Andersson, I. Jex, and C. Silberhorn, *Phys. Rev. Lett.* **104**, 050502 (2010).
- [19] H. Schmitz, R. Matjeschk, C. Schneider, J. Glueckert, M. Enderlein, T. Huber, and T. Schaetz, *Phys. Rev. Lett.* **103**, 090504 (2009).
- [20] A. Kitaev, *AIP Conf. Proc.* **1134**, 22 (2009).
- [21] L. Fidkowski and A. Kitaev, *Phys. Rev. B* **83**, 075103 (2011).
- [22] M. Z. Hasan and C. L. Kane, *Rev. Mod. Phys.* **82**, 3045 (2010).
- [23] R. B. Laughlin, *Phys. Rev. B* **23**, 5632 (1981).
- [24] M. Atala, M. Aidelsburger, J. T. Barreiro, D. Abanin, T. Kitagawa, E. Demler, and I. Bloch, *Nat. Phys.* **9**, 795 (2013).
- [25] M. Aidelsburger, M. Lohse, C. Schweizer, M. Atala, J. T. Barreiro, S. Nascimbène, N. Cooper, I. Bloch, and N. Goldman, *Nat. Phys.* **11**, 162 (2015).
- [26] S. Mittal, S. Ganeshan, J. Fan, A. Vaezi, and M. Hafezi, *Nat. Photonics* **10**, 180 (2016).
- [27] J. M. Zeuner, M. C. Rechtsman, Y. Plotnik, Y. Lumer, S. Nolte, M. S. Rudner, M. Segev, and A. Szameit, *Phys. Rev. Lett.* **115**, 040402 (2015).
- [28] D. A. Abanin, T. Kitagawa, I. Bloch, and E. Demler, *Phys. Rev. Lett.* **110**, 165304 (2013).
- [29] F. Grusdt, D. Abanin, and E. Demler, *Phys. Rev. A* **89**, 043621 (2014).
- [30] M. C. Banuls, C. Navarrete, A. Perez, E. Roldan, and J. C. Soriano, *Phys. Rev. A* **73**, 062304 (2006).
- [31] C. Cedzich, T. Rybar, A.H. Werner, A. Alberti, M. Genske, and R.F. Werner, *Phys. Rev. Lett.* **111**, 160601 (2013).
- [32] C. Cedzich and R.F. Werner, *Phys. Rev. A* **93**, 032329 (2016).
- [33] See Supplemental Material at <http://link.aps.org/supplemental/10.1103/PhysRevLett.118.130501> for details of the derivations.
- [34] Note that there exists a chiral symmetric time frame if one moves half of the first rotation to the end of the walk cycle [10,13,33].
- [35] To be precise, the full topological phase of the split-step quantum walks consists of the bulk winding number defined in the main text measured in two different time frames [13]. Thus, to fully characterize the topological phase of a given quantum walk, our protocol must be performed twice, once in each chiral symmetric time frame.
- [36] We note that refocusing also occurs for dynamical phases that are an odd multiple of  $\pi$ . In such cases, one needs either

- to account for the dynamical phase in the winding number calculation, or double the total number of steps.
- [37] This is analogous to continuous-time evolution, where  $\phi_{\text{dyn}}$  is directly proportional to the time taken to traverse a path in parameter space.
- [38] While a physical interpretation of the dynamical phase is not obvious in the nonadiabatic case, it can be defined formally by solving the Schrödinger equation neglecting the band-mixing term, as is done in the Supplemental Material [33].
- [39] A. Blais, R.-S. Huang, A. Wallraff, S. M. Girvin, and R. J. Schoelkopf, *Phys. Rev. A* **69**, 062320 (2004).
- [40] J. Koch, T. M. Yu, J. Gambetta, A. A. Houck, D. I. Schuster, J. Majer, A. Blais, M. H. Devoret, S. M. Girvin, and R. J. Schoelkopf, *Phys. Rev. A* **76**, 042319 (2007).
- [41] B. C. Travaglione and G. J. Milburn, *Phys. Rev. A* **65**, 032310 (2002).
- [42] P. Xue, B. C. Sanders, A. Blais, and K. Lalumière, *Phys. Rev. A* **78**, 042334 (2008).
- [43] Z. Chen *et al.*, *Phys. Rev. Lett.* **116**, 020501 (2016).
- [44] D. I. Schuster, A. A. Houck, J. A. Schreier, A. Wallraff, J. M. Gambetta, A. Blais, L. Frunzio, J. Majer, B. Johnson, M. H. Devoret, S. M. Girvin, and R. J. Schoelkopf, *Nature (London)* **445**, 515 (2007).
- [45] B. Vlastakis, G. Kirchmair, Z. Leghtas, S. E. Nigg, L. Frunzio, S. M. Girvin, M. Mirrahimi, M. H. Devoret, and R. J. Schoelkopf, *Science* **342**, 607 (2013).
- [46] M. J. Peterer, S. J. Bader, X. Jin, F. Yan, A. Kamal, T. J. Gudmundsen, P. J. Leek, T. P. Orlando, W. D. Oliver, and S. Gustavsson, *Phys. Rev. Lett.* **114**, 010501 (2015).
- [47] By using a single local oscillator to perform both excitation into and out of the  $|f\rangle$  state, the evolved dynamical phase associated with this state is automatically kept track of and canceled.
- [48] E. Flurin, V. V. Ramasesh, S. Hacoheh-Gourgy, L. S. Martin, N. Y. Yao, and I. Siddiqi, [arXiv:1610.03069](https://arxiv.org/abs/1610.03069).